

Supporting Information Materials

for

**2,2'-Disilylazobenzenes Featuring Intramolecular Double Nitrogen···Silicon Coordination:  
A Photoisomerizable Fluorophore**

Naokazu Kano,\* Masaki Yamamura and Takayuki Kawashima\*

Department of Chemistry, Graduate School of Science, The University of Tokyo, 7-3-1 Hongo,  
Bunkyo-ku, Tokyo 113-0033, Japan

**Contents**

- S2 NMR spectral charts of (*E*)-**4a-e** and (*Z*)-**4a,d,e**
- S10 Change of UV-vis absorption spectra of (*E*)- and (*Z*)-**4a-e** upon photoirradiation
- S15 Change of fluorescence spectra of (*E*)- and (*Z*)-**4e** upon photoirradiation
- S16 TD-DFT calculations of (*E*)-**4e**, (*E*)-**5**, and (*E*)-**6**

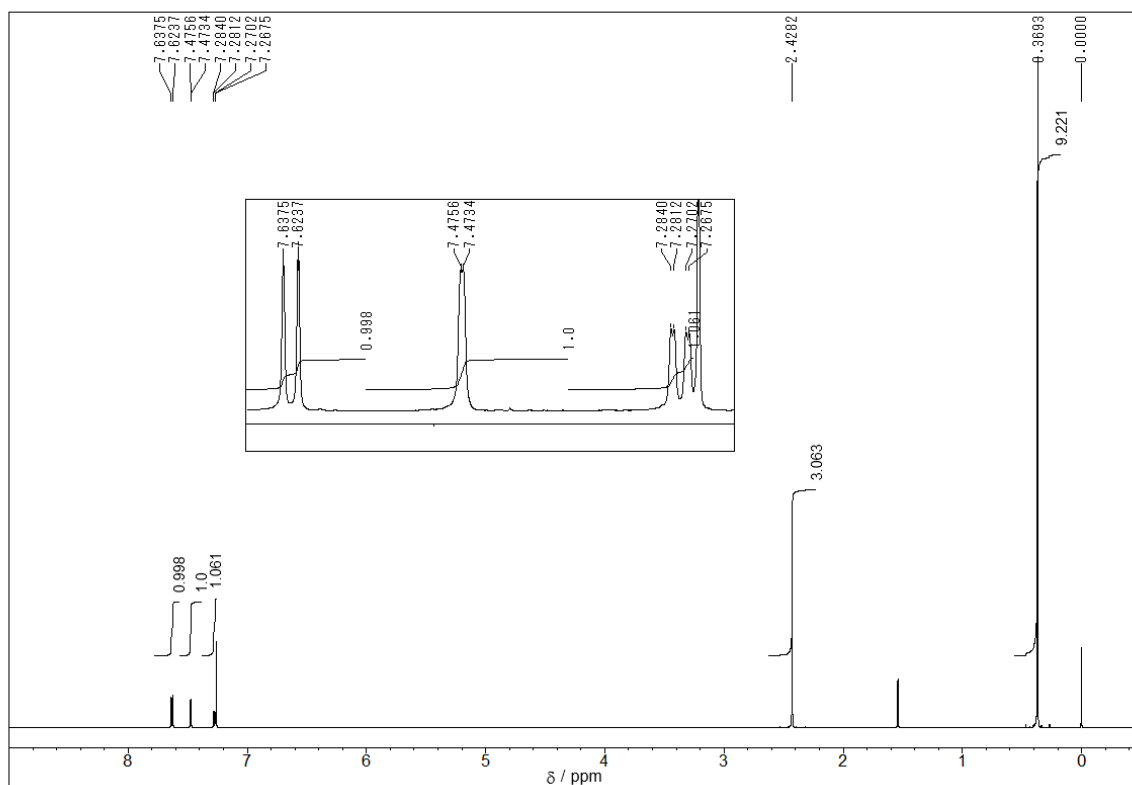


Figure S1.  $^1\text{H}$  NMR spectrum of (*E*)-**4a** in  $\text{CDCl}_3$  (600 MHz).

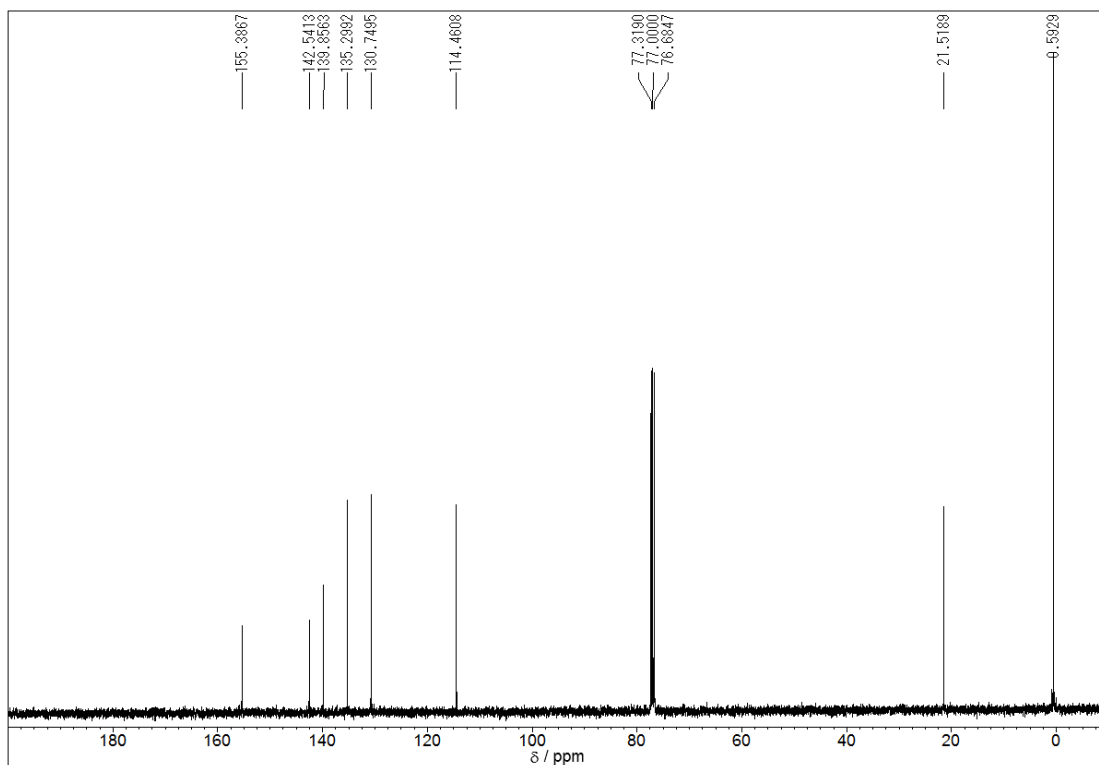


Figure S2.  $^{13}\text{C}$  NMR spectrum of (*E*)-**4a** in  $\text{CDCl}_3$  (100 MHz).

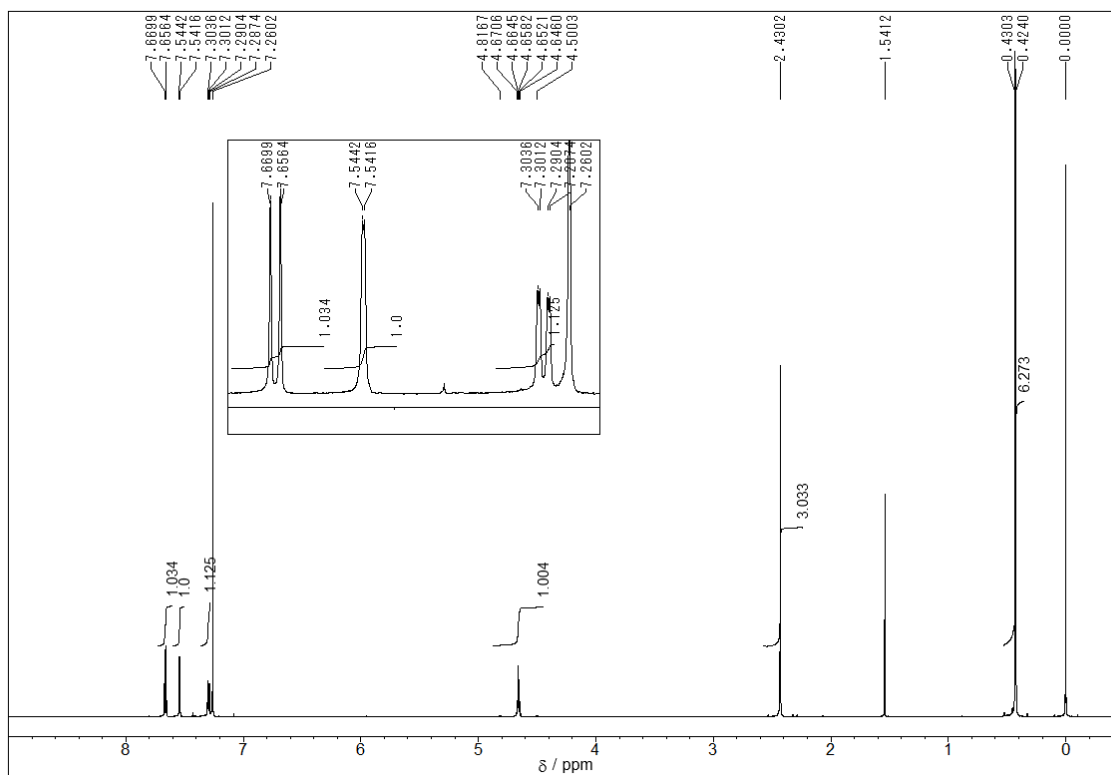


Figure S3.  $^1\text{H}$  NMR spectrum of (*E*)-**4b** in  $\text{CDCl}_3$  (600 MHz).

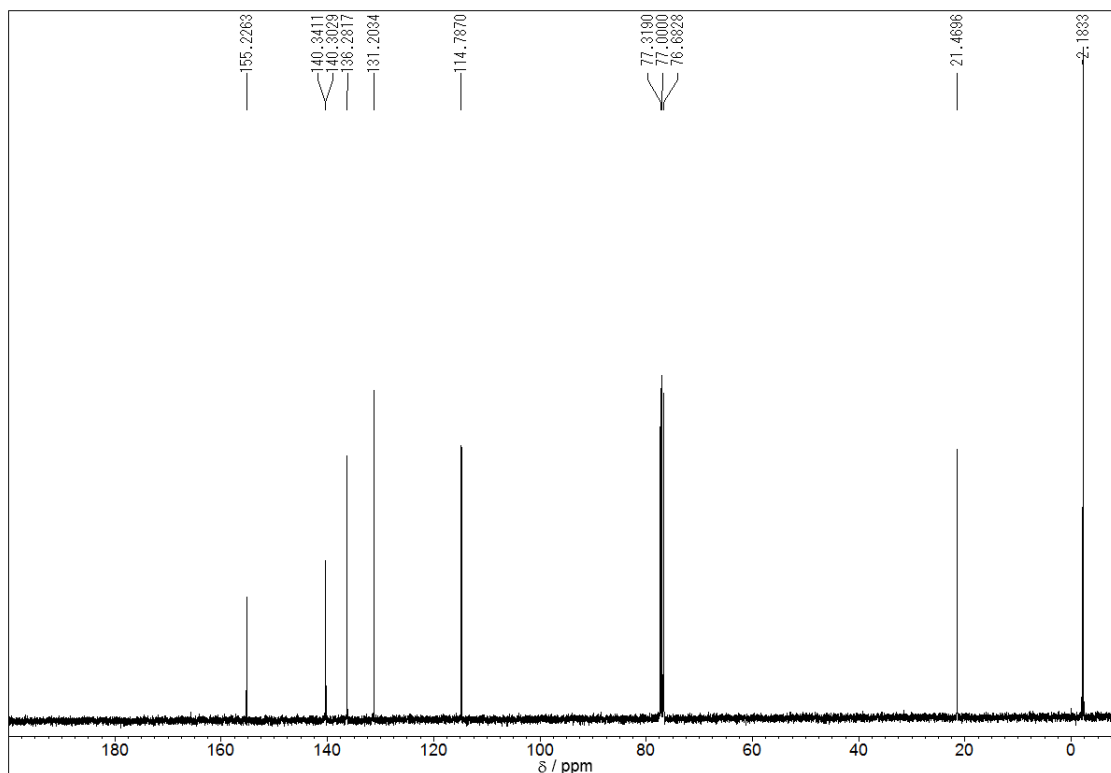


Figure S4.  $^{13}\text{C}$  NMR spectrum of (*E*)-**4b** in  $\text{CDCl}_3$  (100 MHz).

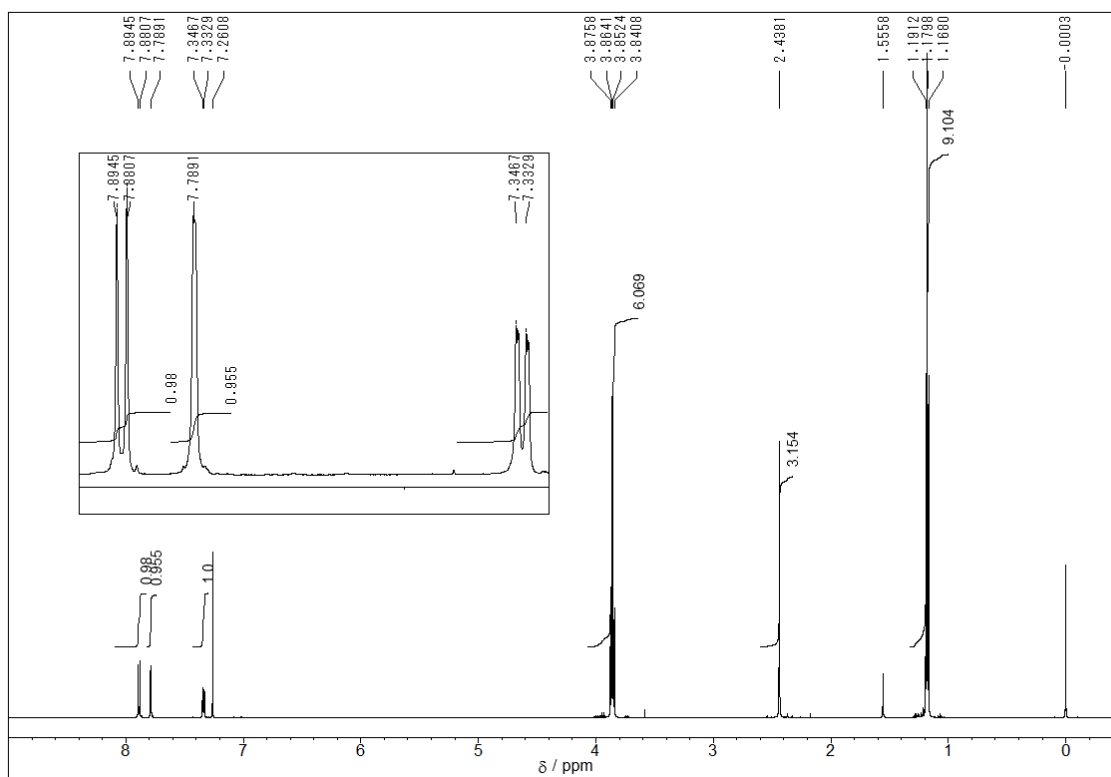


Figure S5.  $^1\text{H}$  NMR spectrum of (*E*)-**4c** in  $\text{CDCl}_3$  (600 MHz).

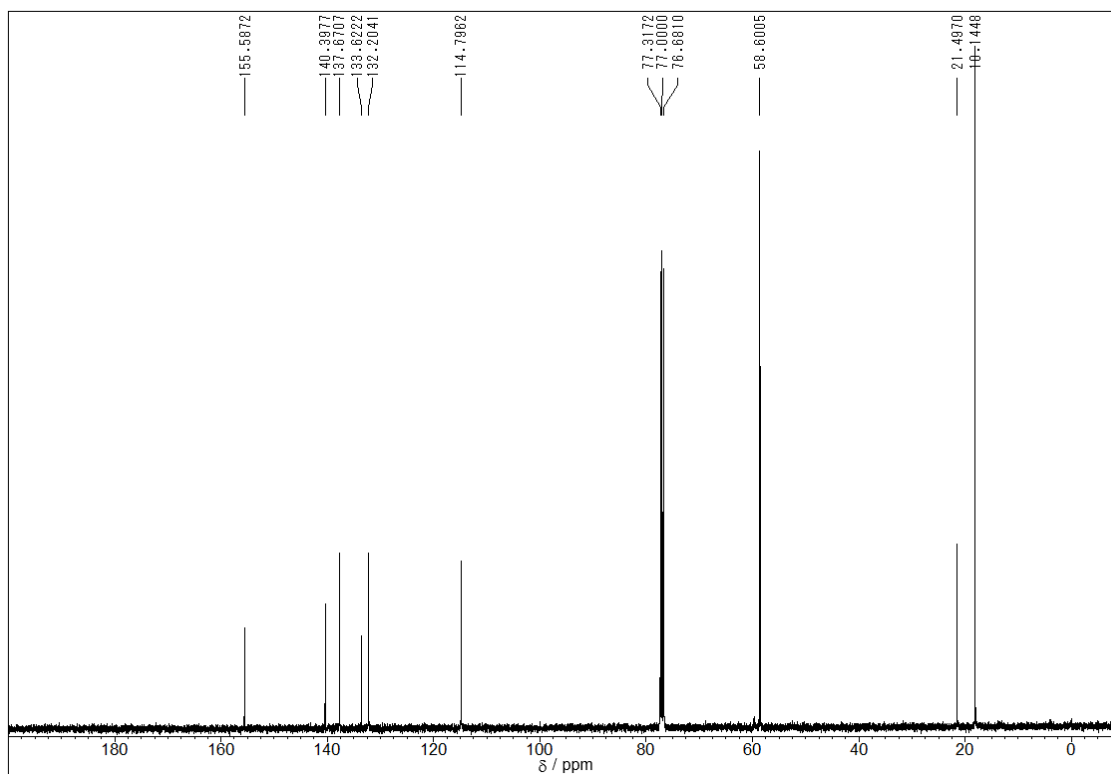


Figure S6.  $^{13}\text{C}$  NMR spectrum of (*E*)-**4c** in  $\text{CDCl}_3$  (100 MHz).

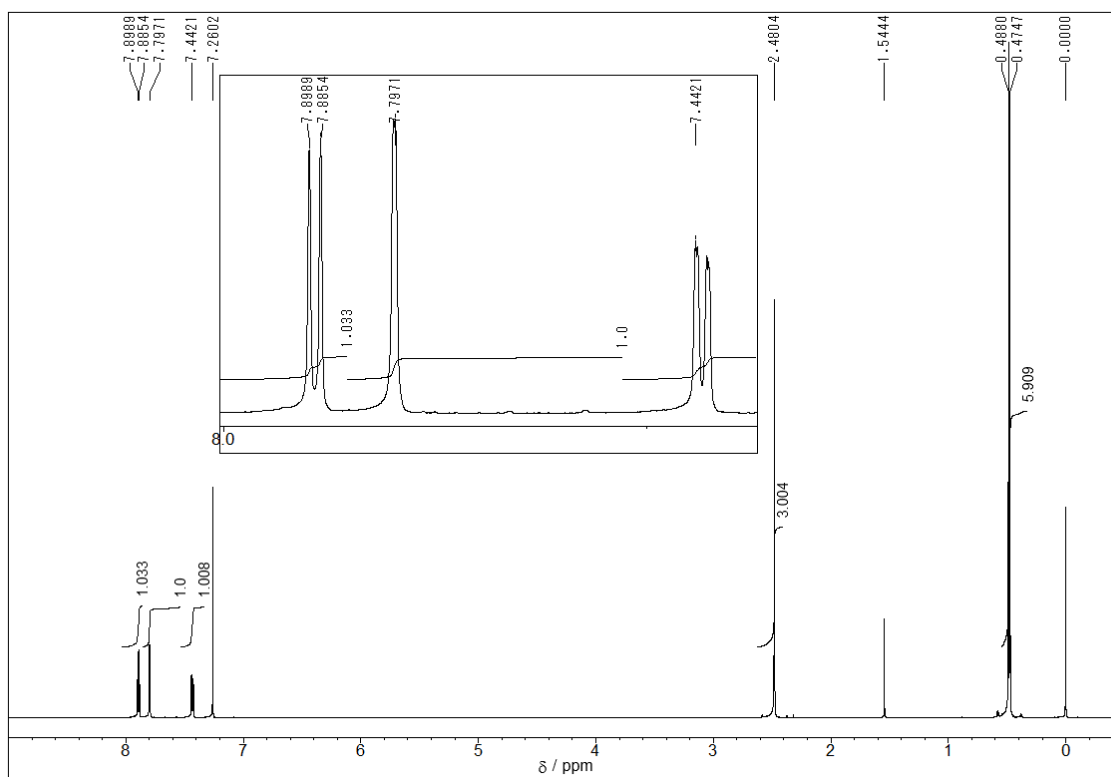


Figure S7.  $^1\text{H}$  NMR spectrum of (*E*)-**4d** in  $\text{CDCl}_3$  (600 MHz).

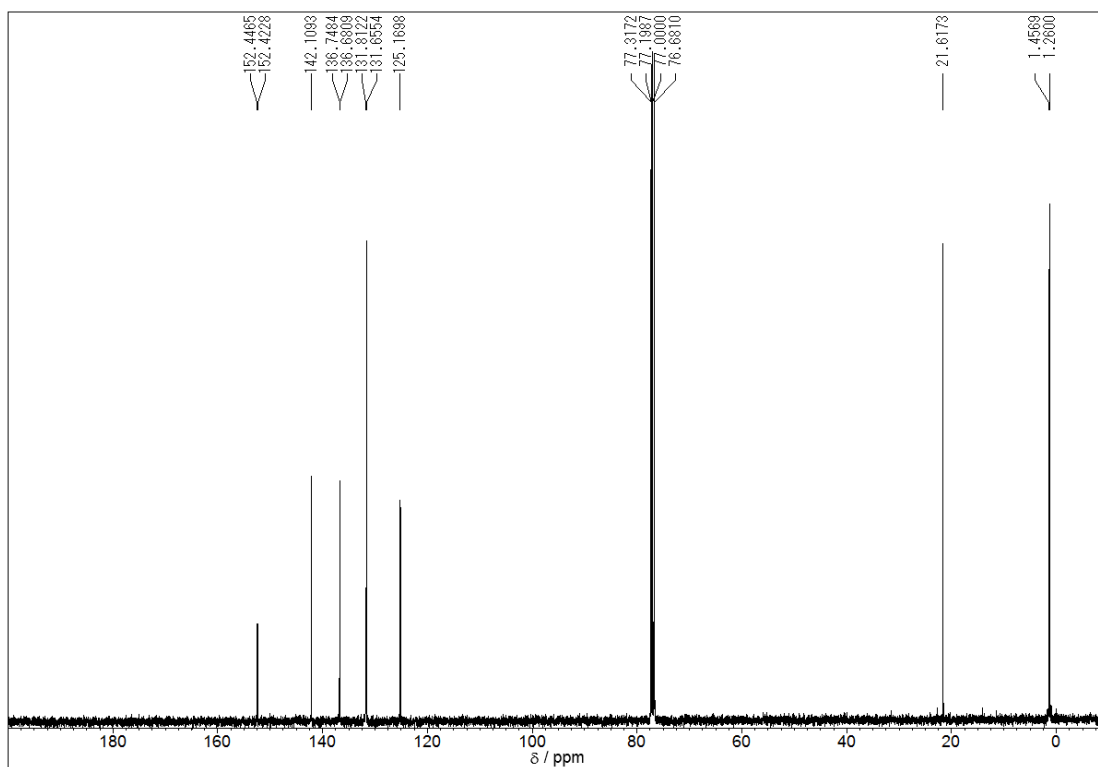


Figure S8.  $^{13}\text{C}$  NMR spectrum of (*E*)-**4d** in  $\text{CDCl}_3$  (100 MHz).

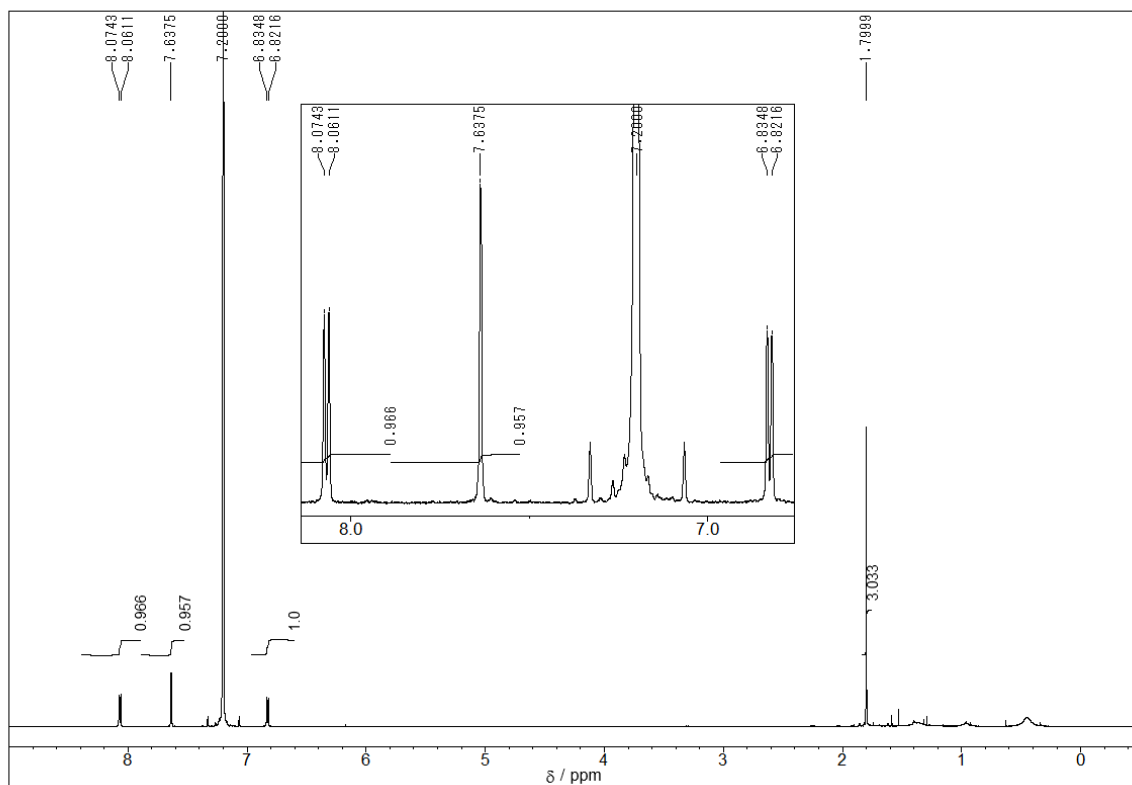


Figure S9.  $^1\text{H}$  NMR spectrum of (*E*)-**4e** in  $\text{C}_6\text{D}_6$  (600 MHz).

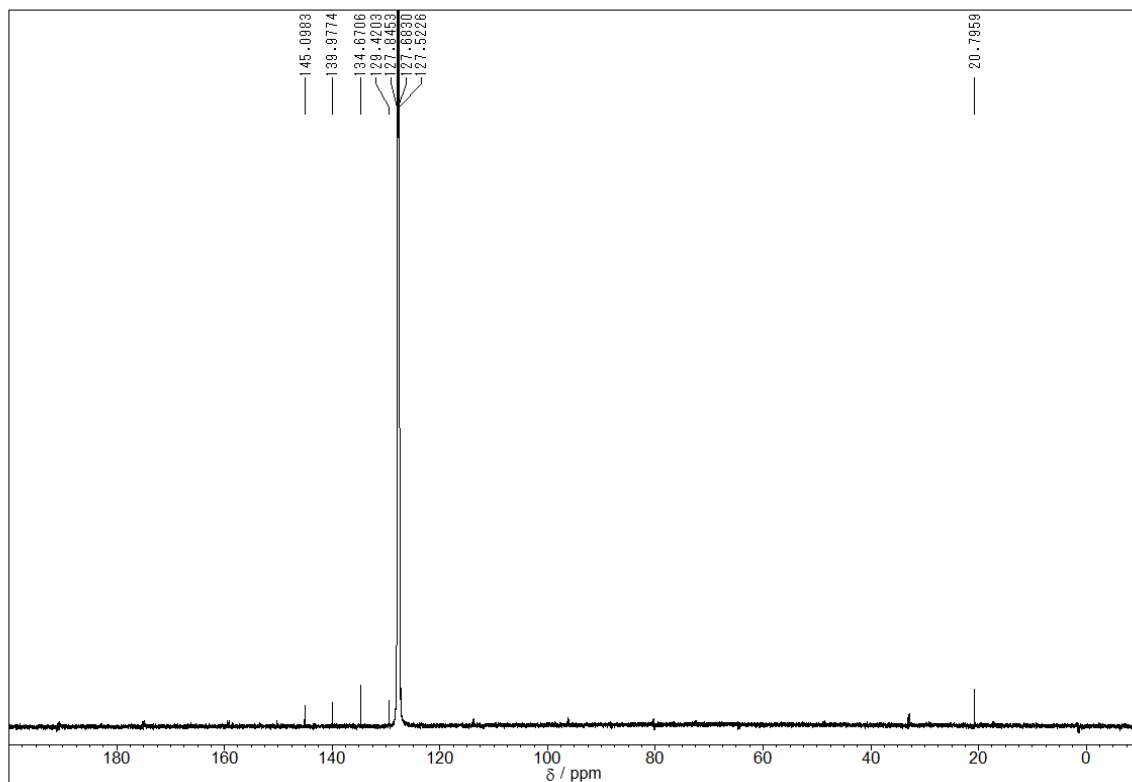


Figure S10.  $^{13}\text{C}$  NMR spectrum of (*E*)-**4e** in  $\text{C}_6\text{D}_6$  (150 MHz).

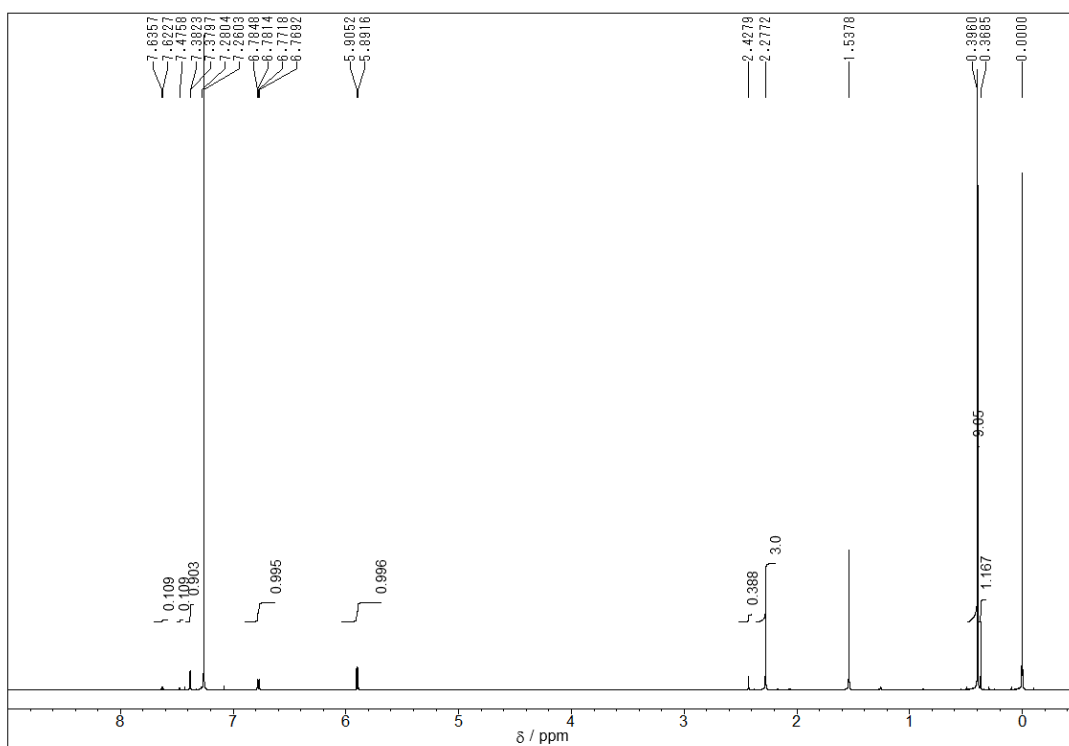


Figure S11. <sup>1</sup>H NMR spectrum of a mixture of (*E*)- and (*Z*)-**4a** in 11/89 ratio in CDCl<sub>3</sub> after photoisomerization.

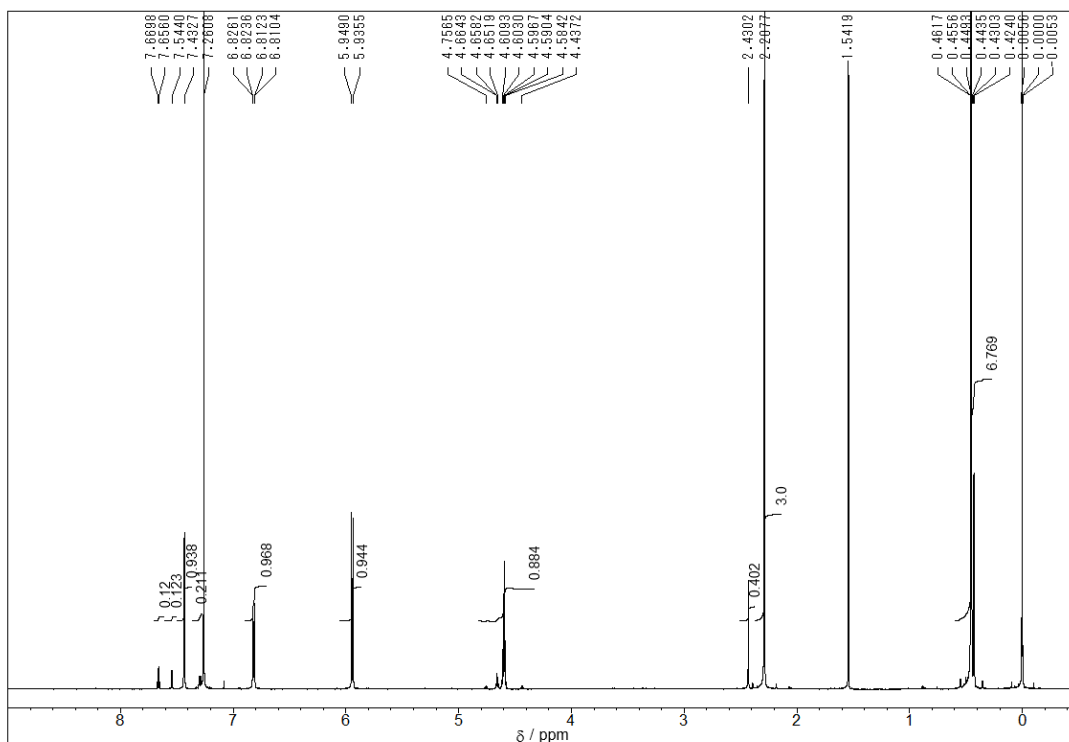


Figure S12. <sup>1</sup>H NMR spectrum of a mixture of (*E*)- and (*Z*)-**4b** in 12/88 ratio in CDCl<sub>3</sub> after photoisomerization.

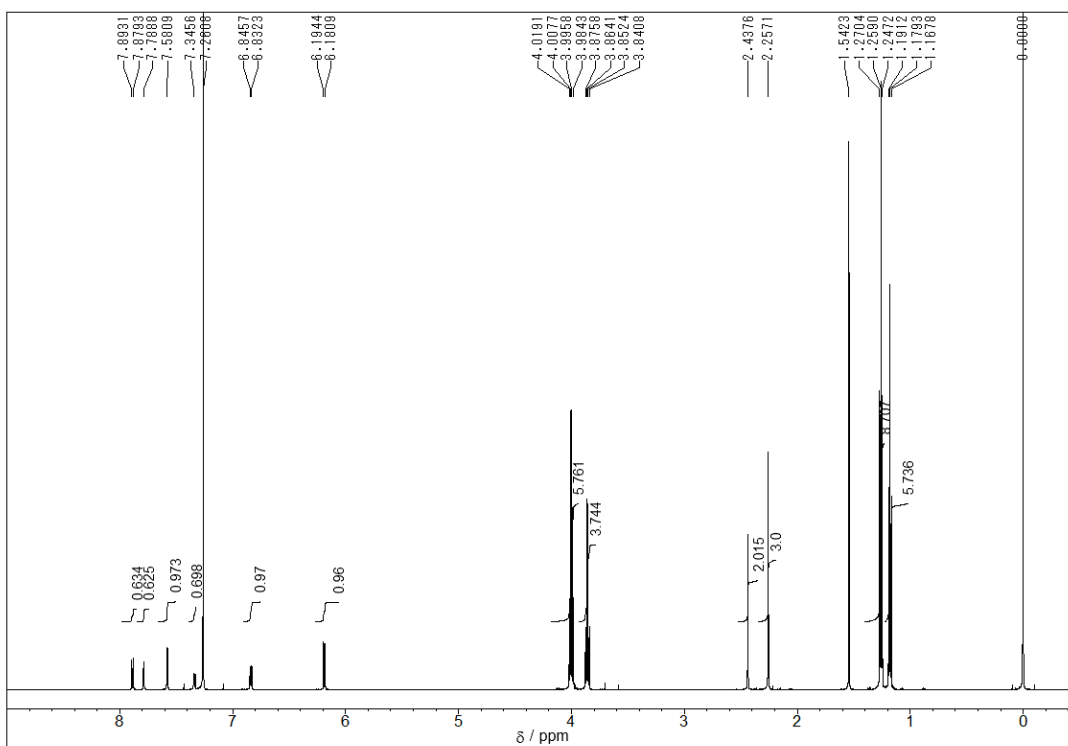


Figure S13.  $^1\text{H}$  NMR spectrum of a mixture of (*E*)- and (*Z*)-**4c** in 40/60 ratio in  $\text{CDCl}_3$  after photoisomerization.

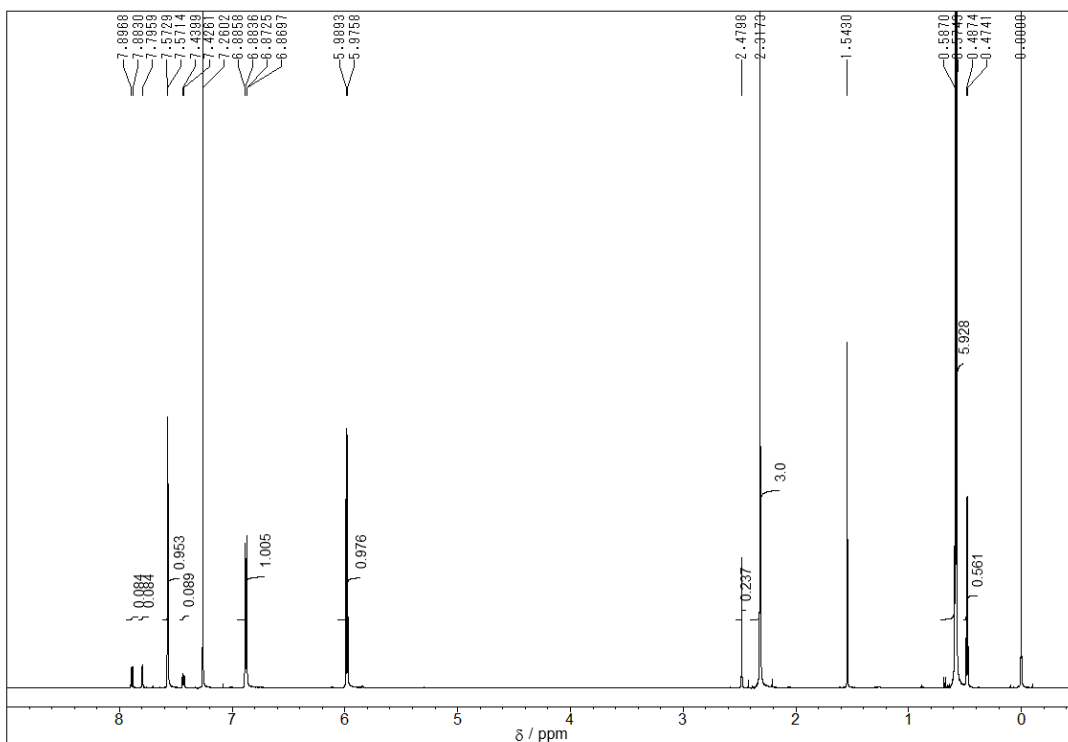


Figure S14.  $^1\text{H}$  NMR spectrum of a mixture of (*E*)- and (*Z*)-**4d** in 7/93 ratio in  $\text{CDCl}_3$  after photoisomerization.



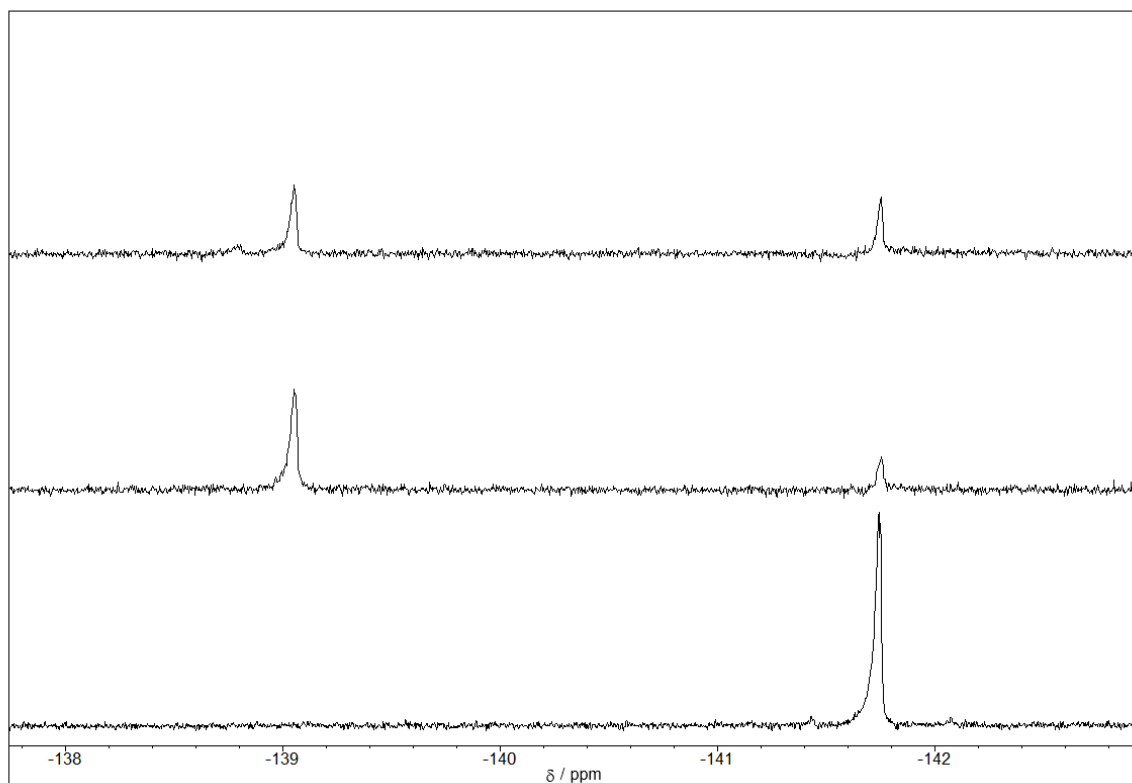


Figure S15.  $^{19}\text{F}$  NMR spectrum of a mixture of (*E*)- and (*Z*)-**4e** in hexane ( $\text{C}_6\text{D}_6$ ) after photoisomerization. Bottom: initial state (only (*E*)-**4e**), middle: photostationary state at 365 nm (a mixture of (*E*)- and (*Z*)-**4e** in 21/79 ratio), and top: photostationary state at 436 nm (a mixture of (*E*)- and (*Z*)-**4e** in 40/60 ratio).

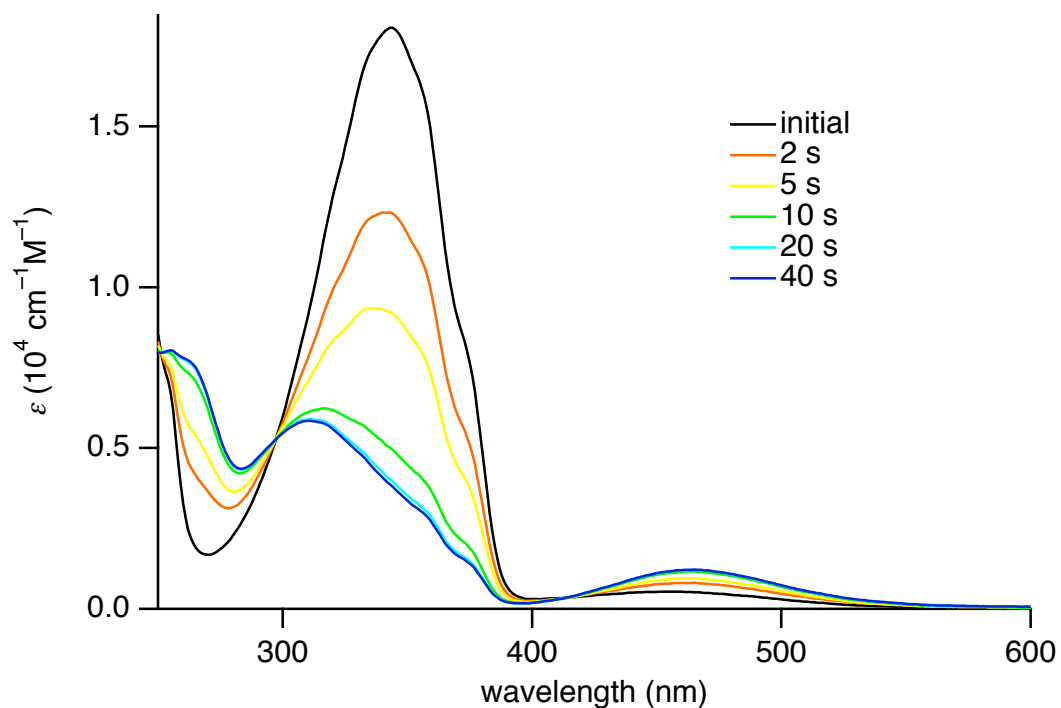


Figure S16. UV-vis absorption spectral change of (*E*)-**4a** upon photoirradiation (hexane, Hg-lamp, 400 W, 365 nm).

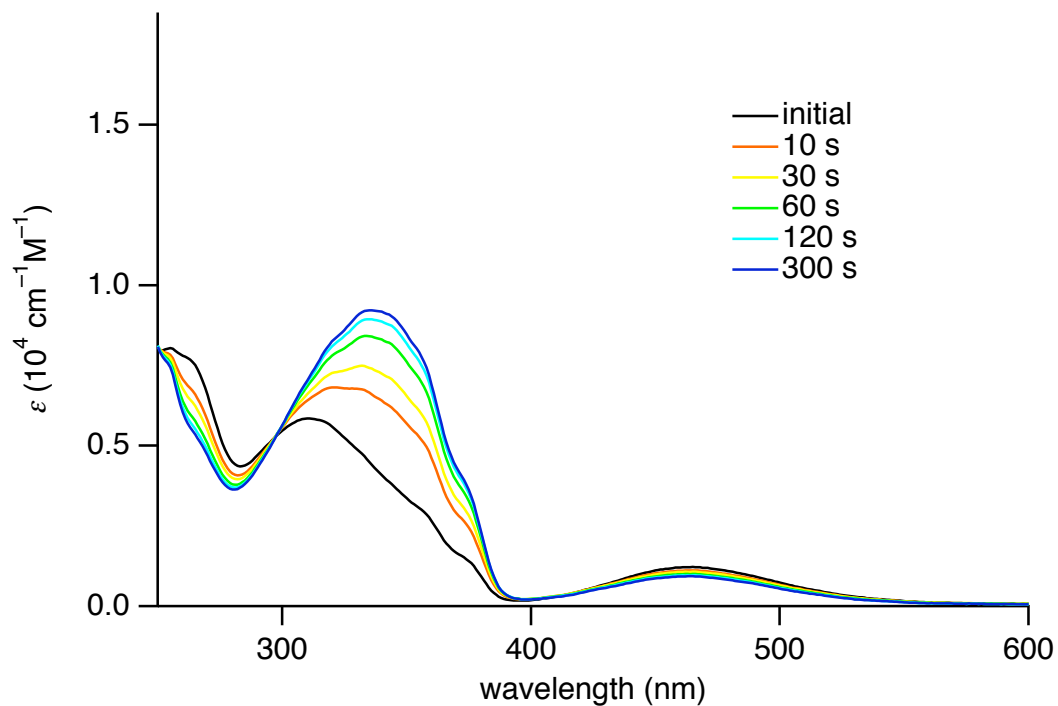


Figure S17. UV-vis absorption spectral change of (*Z*)-**4a** (PPS at 365 nm) upon photoirradiation (hexane, Hg-lamp, 400 W, 436 nm).

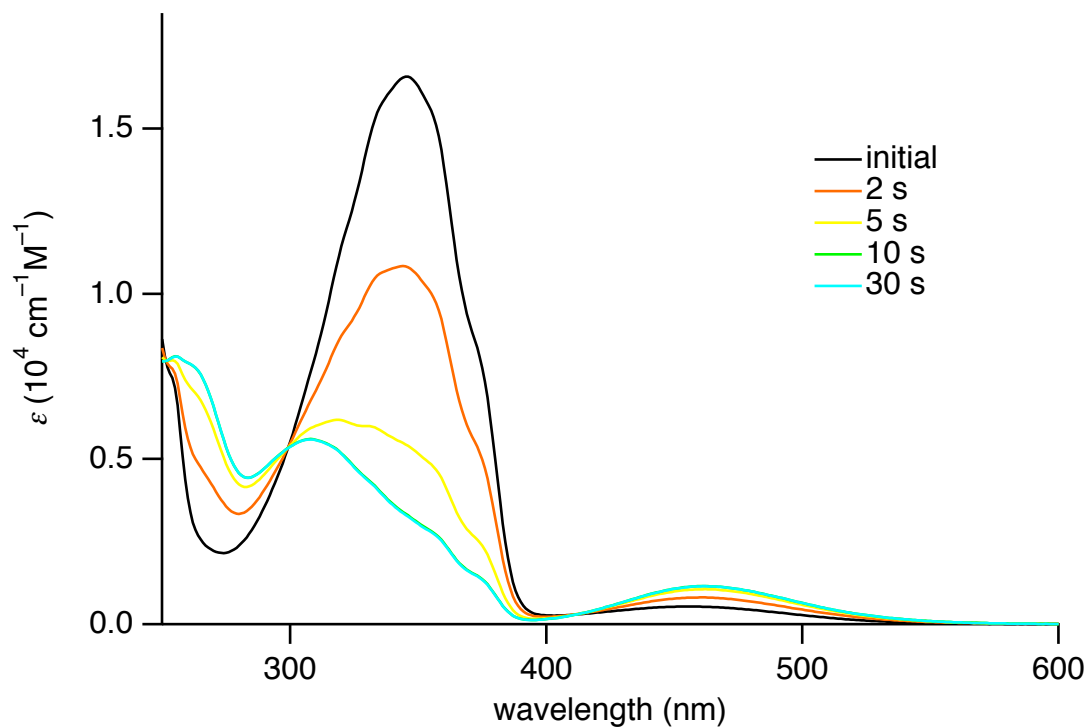


Figure S18. UV-vis absorption spectral change of (*E*)-**4b** upon photoirradiation (hexane, Hg-lamp, 400 W, 365 nm).

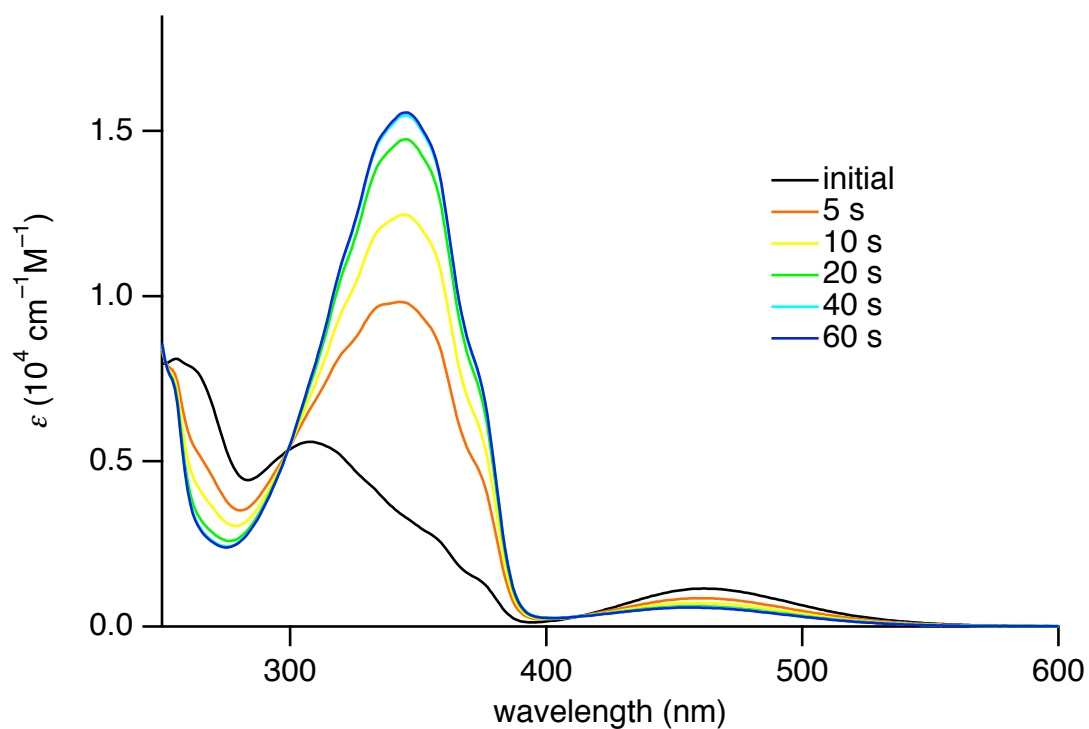


Figure S19. UV-vis absorption spectral change of (*Z*)-**4b** (PPS at 365 nm) upon photoirradiation (hexane, Hg-lamp, 400 W, 436 nm).

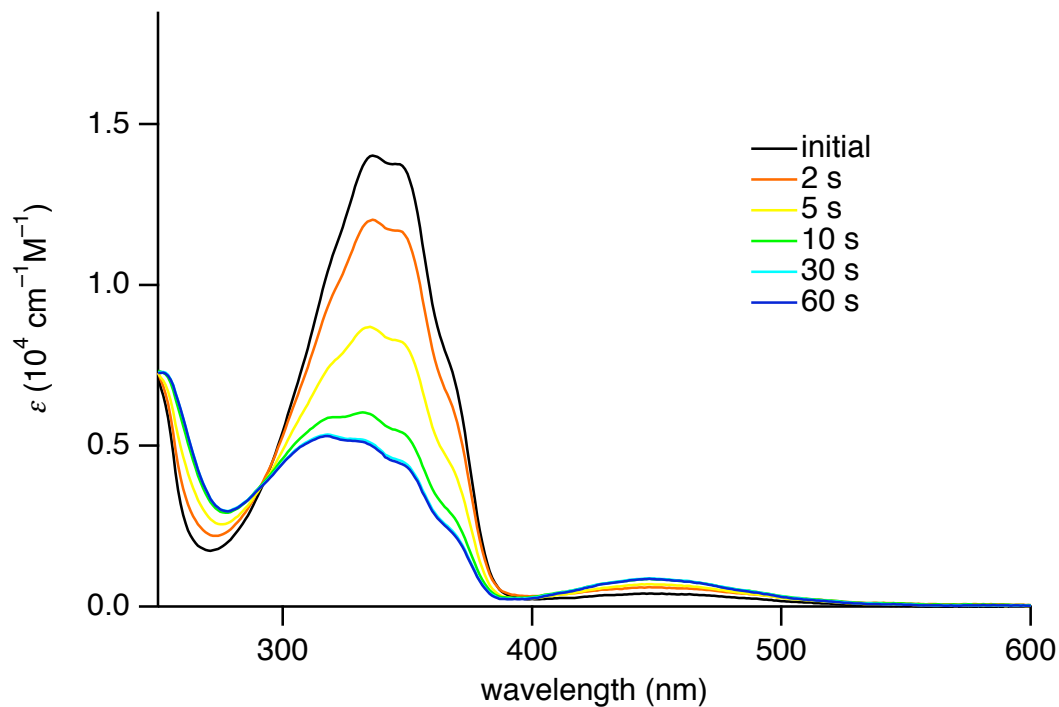


Figure S20. UV-vis absorption spectral change of (*E*)-**4c** upon photoirradiation (hexane, Hg-lamp, 400 W, 365 nm).

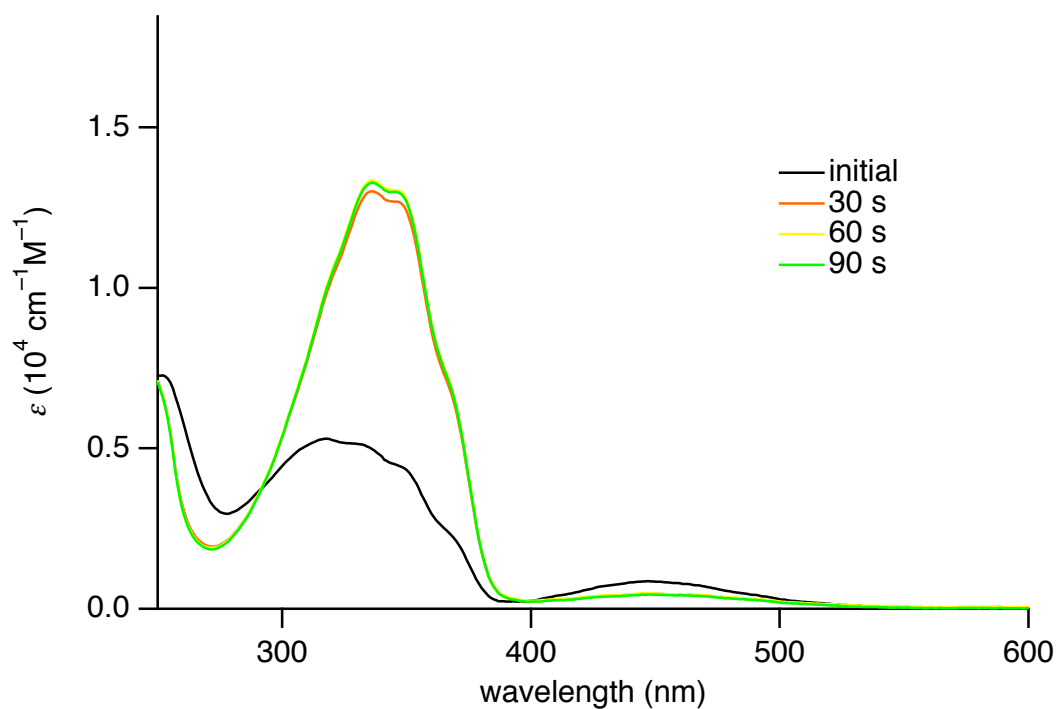


Figure S21. UV-vis absorption spectral change of (*Z*)-**4c** (PPS at 365 nm) upon photoirradiation (hexane, Hg-lamp, 400 W, 436 nm).

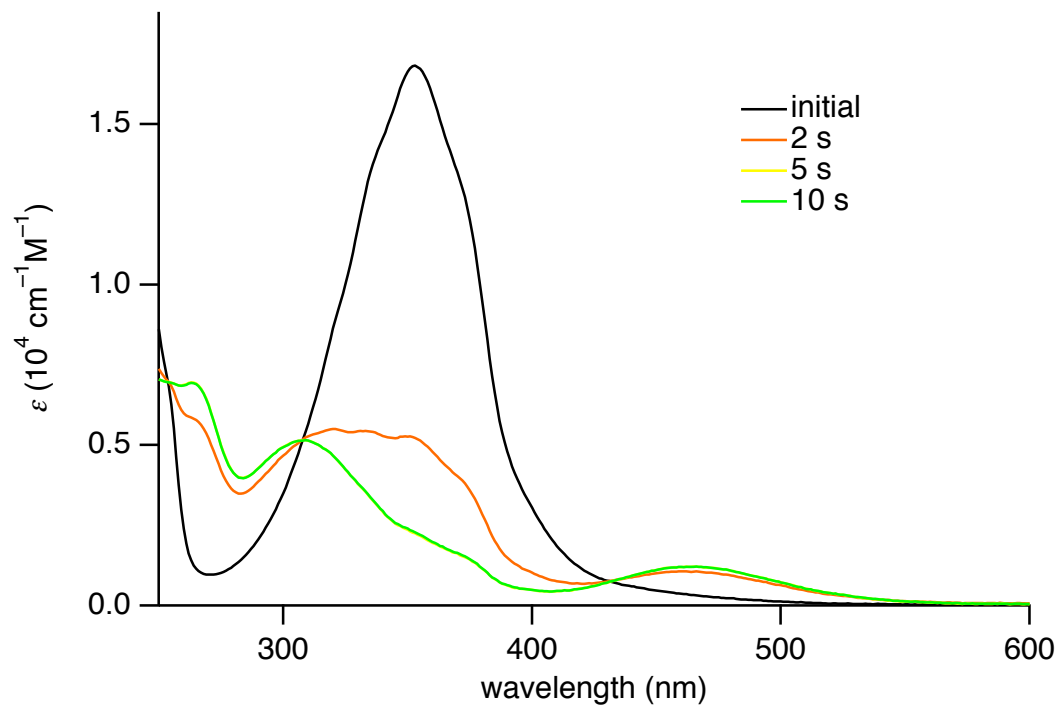


Figure S22. UV-vis absorption spectral change of (*E*)-**4d** upon photoirradiation (hexane, Hg-lamp, 400 W, 365 nm).

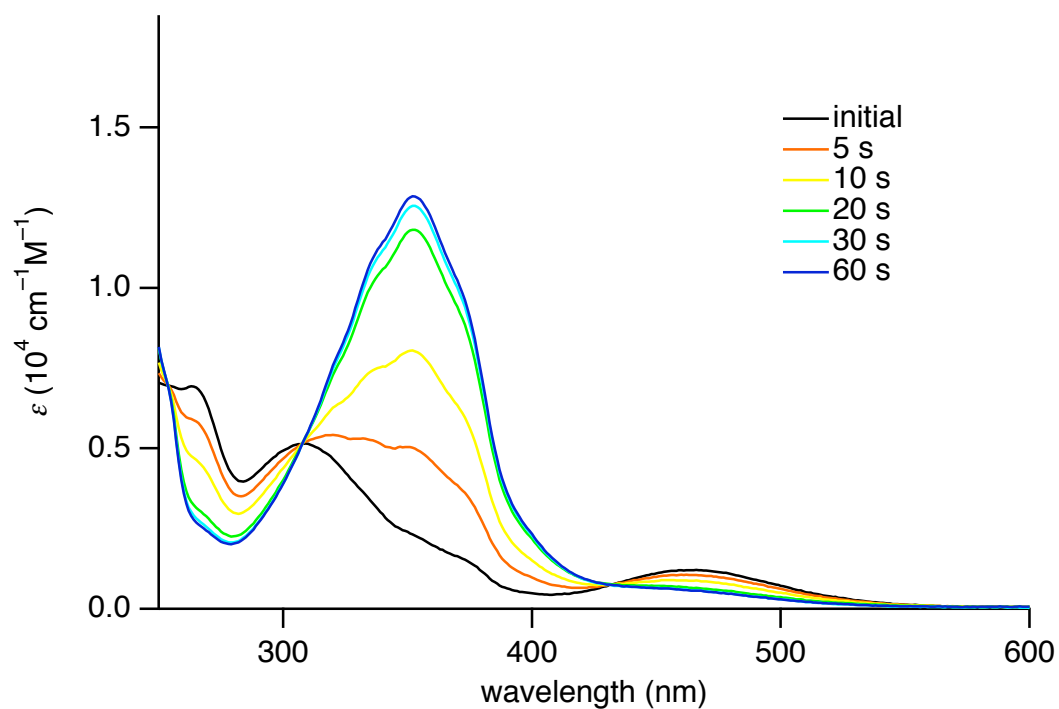


Figure S23. UV-vis absorption spectral change of (*Z*)-**4d** (PPS at 365 nm) upon photoirradiation (hexane, Hg-lamp, 400 W, 436 nm).

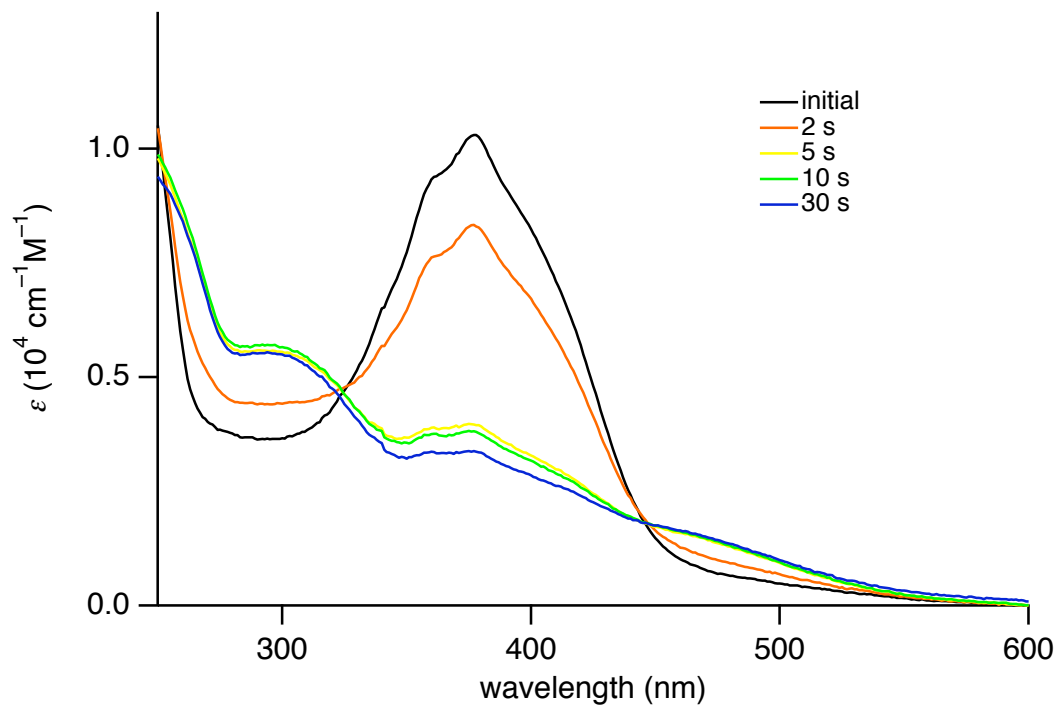


Figure S24. UV-vis absorption spectral change of (*E*)-**4e** upon photoirradiation (hexane, Hg-lamp, 400 W, 365 nm).

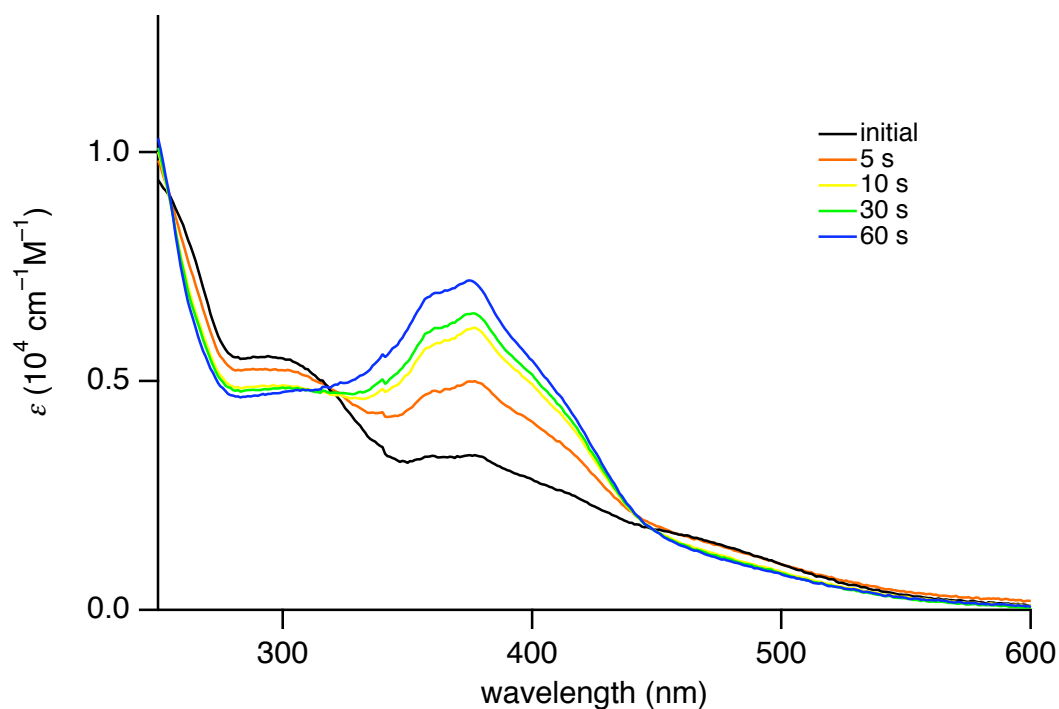


Figure S25. UV-vis absorption spectral change of (*Z*)-**4e** (PPS at 365 nm) upon photoirradiation (hexane, Hg-lamp, 400 W, 436 nm).

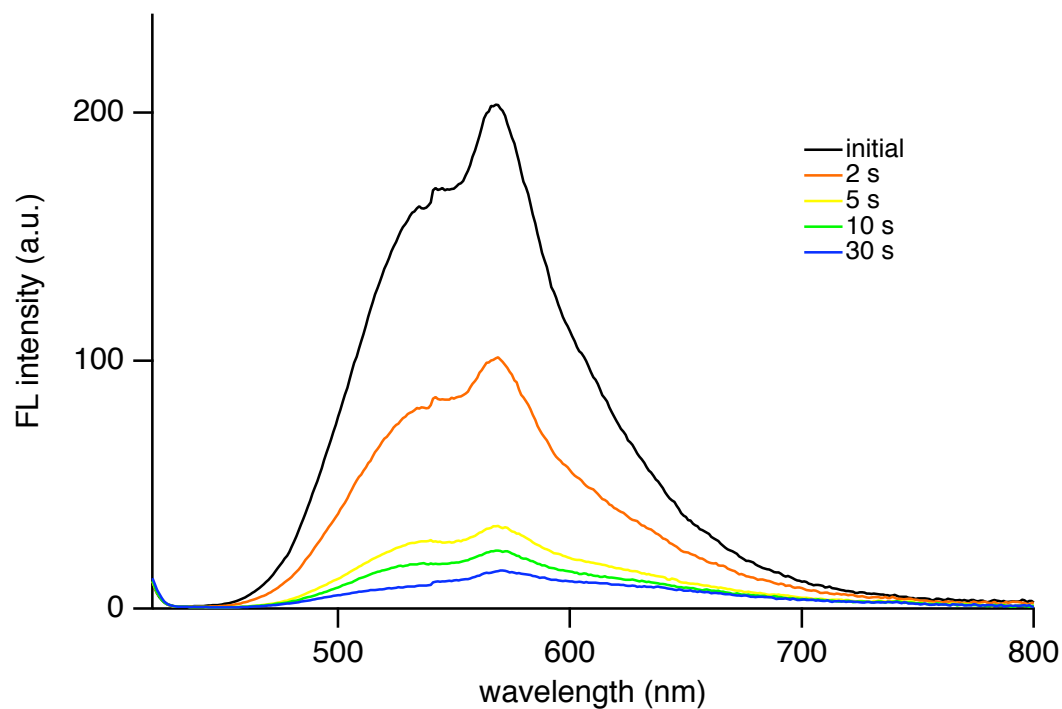


Figure S26. Fluorescence spectral change of (*E*)-**4e** upon photoirradiation (hexane,  $\lambda_{\text{ex}} = 380$  nm, Hg-lamp, 400 W, 365 nm).

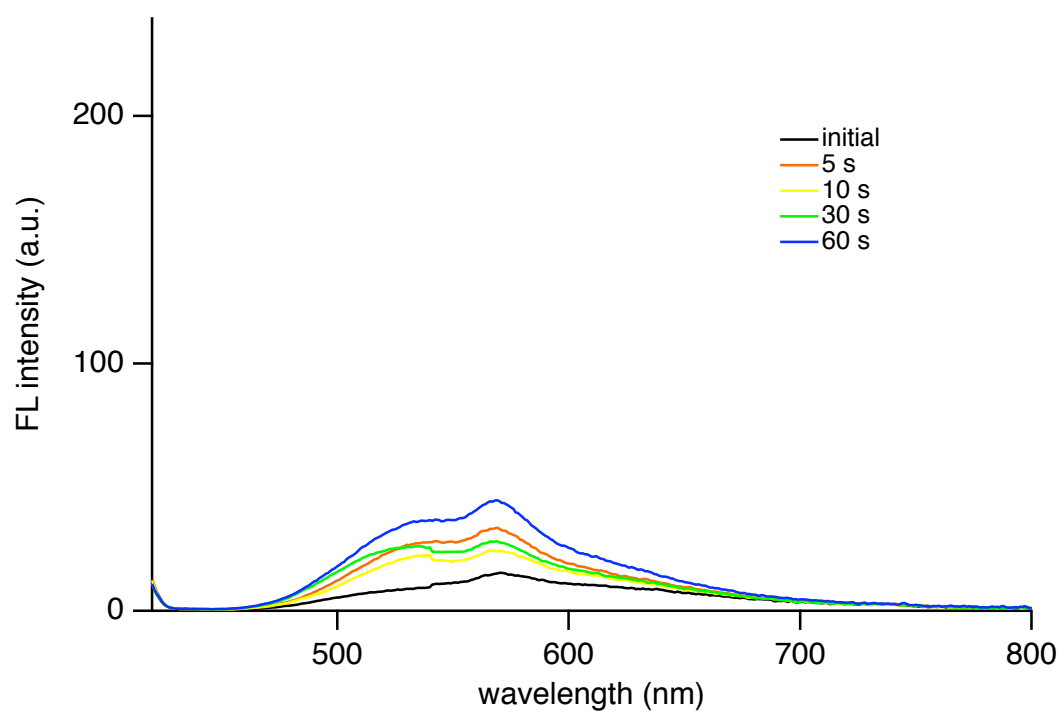


Figure S27. Fluorescence spectral change of (*Z*)-**4e** (PPS at 365 nm) upon photoirradiation (hexane,  $\lambda_{\text{ex}} = 380$  nm, Hg-lamp, 400 W, 436 nm).

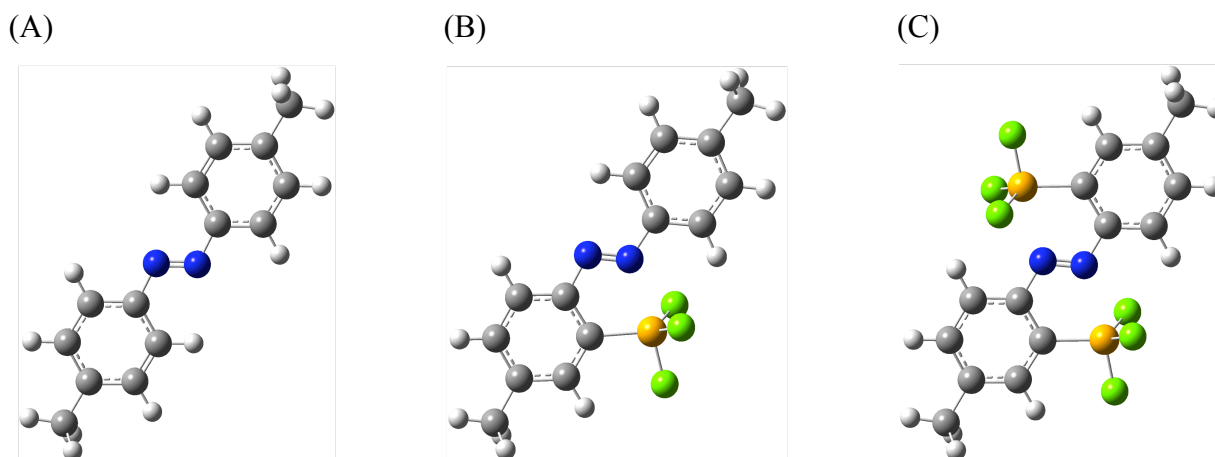


Figure S28. Optimized structures of (A) (*E*)-**5**, (B) (*E*)-**6**, and (C) (*E*)-**4e**. (Magenta: silicon; gray: carbon; yellow-green: fluorine; white: hydrogen; blue: nitrogen).

Table S1. Singlet excited energies of (*E*)-**5**, (*E*)-**6**, and (*E*)-**4e** calculated at the B3PW91/6-311++G(2d,p) level.

		transition (assignment is in parentheses)	excitation energy / eV (oscillator strength, <i>f</i> )
<b>(E)-5</b>	S <sub>1</sub>	HOMO-1 → LUMO (n,π*)	2.60 (0.0000)
	S <sub>2</sub>	HOMO → LUMO (π,π*)	3.54 (0.9510)
<b>(E)-6</b>	S <sub>1</sub>	HOMO-1 → LUMO (n,π*)	2.99 (0.0009)
	S <sub>2</sub>	HOMO → LUMO (π,π*)	3.21 (0.7416)
<b>(E)-4e</b>	S <sub>1</sub>	HOMO → LUMO (π,π*)	3.02 (0.6421)
	S <sub>2</sub>	HOMO-3 → LUMO (n,π*)	3.18 (0.0000)